

Discovery of Imidazopyridines as Potent Inhibitors of Indoleamine 2,3-Dioxygenase 1 for Cancer Immunotherapy

Liping Zhang,* Emily C. Cherney,* Xiao Zhu, Tai-an Lin, Johnni Gullo-Brown, Derrick Maley, Kathy Johnston-Allegretto, Lisa Kopcho, Mark Fereshteh, Christine Huang, Xin Li, Sarah C. Traeger, Gopal Dhar, Aravind Anandam, Sandeep Mahankali, Shweta Padmanabhan, Prabhakar Rajanna, Venkata Murali, Thanga Mariappan, Robert Borzilleri, Gregory Vite, John T. Hunt, and Aaron Balog*

Cite This: *ACS Med. Chem. Lett.* 2021, 12, 494–501

Read Online

ACCESS |

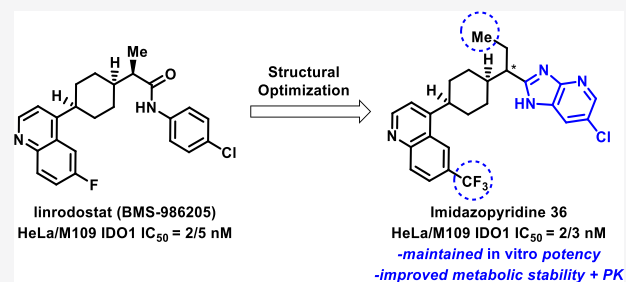
Metrics & More

Article Recommendations

Supporting Information

ABSTRACT: Indoleamine 2,3-dioxygenase 1 (IDO1) has been identified as a target for small-molecule immunotherapy for the treatment of a variety of cancers including renal cell carcinoma and metastatic melanoma. This work focuses on the identification of IDO1 inhibitors containing replacements or isosteres for the amide found in BMS-986205, an amide-containing, IDO1-selective inhibitor currently in phase III clinical trials. Detailed subsequently are efforts to identify a structurally differentiated IDO1 inhibitor via the pursuit of a variety of heterocyclic isosteres, leading to the discovery of highly potent, imidazopyridine-containing IDO1 inhibitors.

KEYWORDS: Indoleamine 2,3-dioxygenase 1, IDO1, immuno-oncology, amide isostere



The clinical success of monoclonal antibody checkpoint inhibitors such as Yervoy (Bristol Myers Squibb, BMS),

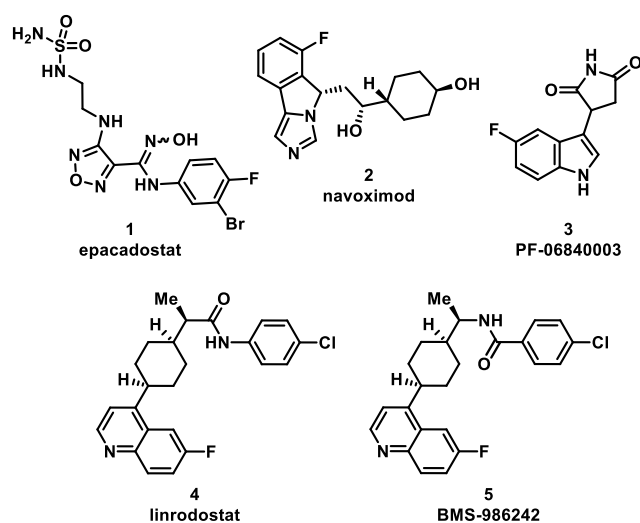


Figure 1. IDO1 inhibitors evaluated in clinical trials.

Keytruda (Merck), and Opdivo (BMS) has received much attention in the field of immuno-oncology (IO). These IO therapies leverage a patient's native immune system to reverse tumor-induced immune suppression and enhance immune response toward cancer.¹ More recently, the effect of metabolism, including amino acid catabolism, on immune

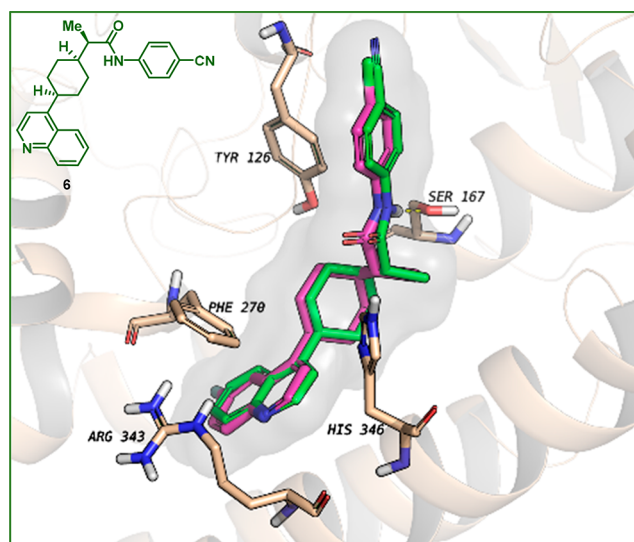


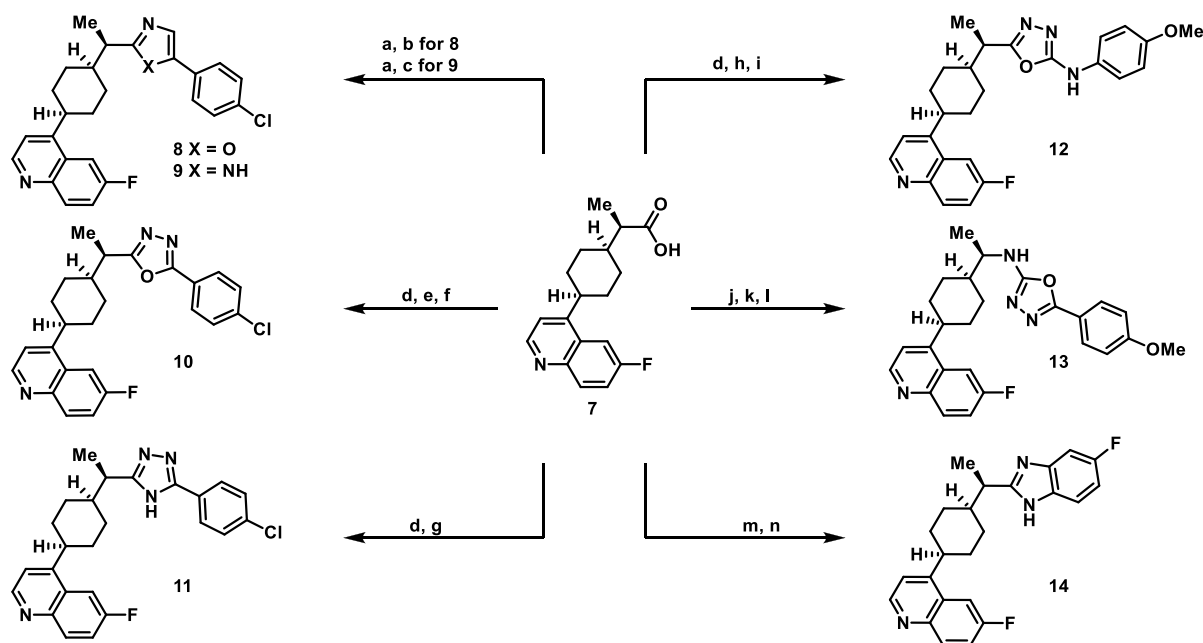
Figure 2. Putative binding mode of 4 (magenta) in hIDO1, based on an X-ray cocrystal structure of compound 6 (green).

Received: January 12, 2021

Accepted: February 26, 2021

Published: March 2, 2021



Scheme 1. Synthesis of Heterocyclic Amide Isosteres and Replacements Starting from Common Intermediate Carboxylic Acid 7^a

^aReagents and conditions: (a) HATU, NMM, 2-amino-1-(4-chlorophenyl)ethan-1-one (64%); (b) POCl₃, 100 °C (56%); (c) NH₄OAc, HOAc, EtOH, 100 °C (17%); (d) (i) HATU, NMM, *tert*-butyl carbazate; (ii) HCl (89% over 2 steps); (e) HATU, NMM, 4-chlorobenzoic acid (83%); (f) POCl₃, 90 °C (55%); (g) pyridine, 4-chlorobenzamide-HCl salt, 110 °C (31%); (h) DIPEA, 1-isocyanato-4-methoxybenzene (93%); (i) POCl₃, 90 °C (26%); (j) DPPA, TEA, toluene, 70 °C; (k) 4-methoxybenzohydrazide, DIPEA (54% over 2 steps); (l) POCl₃, 100 °C (52%); (m) (i) SOCl₂, DMF (ii) CH₂Cl₂, TEA, 4-fluoro-1,2-phenylenediamine, (n) MsOH, 90 °C (50% over 3 steps).

response in the tumor microenvironment (TME) has provided a basis for exploring IO targets capable of perturbation by small molecules. One such strategy for small-molecule cancer immunotherapy involves the inhibition of indoleamine 2,3-dioxygenase 1 (IDO1) to decrease local kynurenine levels in the TME and restore cancer immunity.¹

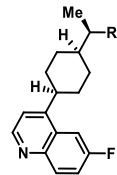
IDO1 is a monomeric, heme-containing dioxygenase enzyme that degrades tryptophan by catalyzing the initial, rate-limiting step of tryptophan metabolism. This step involves the oxidative cleavage of the indole 2,3-double bond of tryptophan to give *N*-formyl kynurenine. Subsequent hydrolysis of *N*-formyl kynurenine yields kynurenine.² IDO1 promotes tumoral immune escape from host immune surveillance and plays an important role in tumor-associated immunosuppression, leading to tolerance toward tumors. Local depletion of tryptophan as well as accumulation of kynurenine have been shown to elicit immunomodulatory activity. Effects include suppression of the T effector (T_{eff}) cell immune response, induction of naïve T cell differentiation into regulatory T (T_{reg}) cells, and both activation of as well as a decrease in dendritic cell (DC) function.³ IDO1 is widely expressed in antigen-presenting cells (DCs, macrophages) and tumor cells, as well as epithelial and vascular endothelial cells. Furthermore, IDO1 can be induced in the tumor microenvironment in response to inflammation and T cell activation following immunotherapy, radiotherapy, or chemotherapy.⁴ This observation is indicative of the potential for IDO1 inhibitors in the context of combination therapies. High IDO1 expression in the tumor or tumor-draining lymph nodes is generally associated with poor prognosis and reduced survival in patients.⁵ Therefore, inhibition of IDO1 is a promising

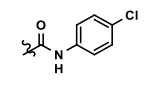
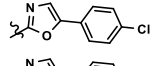
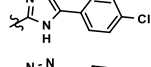
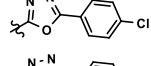
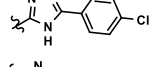
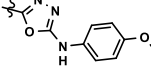
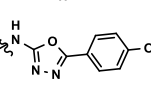
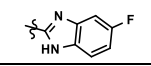
strategy for the re-establishment of immunogenic responses to cancer.

Several IDO1 inhibitors have entered clinical trials for the treatment of cancer (Figure 1).⁶ Epacadostat (INCB24360) (1), an orally active, hydroxyamidine-containing small molecule developed by Incyte, entered Phase III clinical trials in 2017.⁷ Preclinically, epacadostat selectively inhibits IDO1 enzymatic activity and effectively regulates the functions of various immune cells including T cells, natural killer (NK) cells, and DCs.^{8,9} *In vivo*, epacadostat (1) suppressed IDO1 activity in mouse and dog plasma and inhibited tumor growth in a lymphocyte-dependent manner in mice.^{9,10} Results from a phase I/II combination study with epacadostat and ipilimumab in melanoma patients showed a 56% overall response rate among 54 efficacy-evaluable patients and a median progression-free survival of 12.4 months.^{11a} However, a phase III study evaluating the combination of epacadostat and keytruda for the treatment of metastatic melanoma demonstrated no significant improvement in progression-free survival.^{11b,c} Navoximod (2), an imidazoisoindoline compound, was discovered by NewLink Genetics and later licensed to Genentech as GDC-0919. Rights to this molecule were later returned to NewLink after phase I clinical trial results were disclosed.¹² The third candidate, *i*Teos/Pfizer's compound PF-06840003 (3), was dosed as a single agent, once daily, in a phase I study in patients with malignant gliomas.¹³ In January 2018, Pfizer stopped the development of the compound due to a lack of efficacy.¹³

In February 2015, BMS expanded its immuno-oncology pipeline in an agreement with Flexus Biosciences and acquired linrodostat (4, BMS-986205). Preclinically, compound 4 exhibits potent inhibitory activity against IDO1 (human

Table 1. Effects of Heterocyclic Amide Replacements on IDO1 Inhibition Potency and Metabolic Stability



Cmpd #	R	HeLa / M109 IC ₅₀ μM ^a	Metabolic Stability (% rem.) (H / M / R) ^b
4		0.002±0.002/ 0.005±0.002 (N=59)	84/31/86
8		0.495±0.090/ 0.631±0.187	97/78/62
9		0.011±0.002/ 0.080±0.005	58/59/3
10		0.239±0.115/ 0.384±0.001	68/41/23
11		0.020±0.005/ 0.286±0.050	88/69/82
12		0.165±0.059/ 0.451±0.096	18/2/0.4
13		0.003 ±0.002/ 0.014±0.006 (N= 3)	64/17/35
14		0.003±0.001/ 0.022±0.021	42/5/0

^aData reported as average test results ($N = 2$, unless otherwise noted). See [Supporting Information](#) for a description of assay conditions.

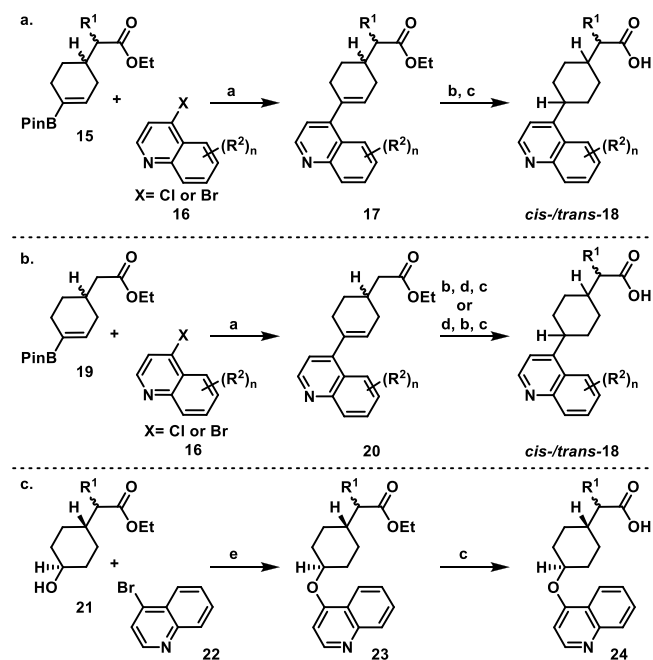
^bFraction of the parent compound (0.5 μM) remaining after a 10 min incubation with 1 mg/mL of human, mouse, and rat liver microsomes (HLM, MsLM, RLM).

HeLa cellular IC₅₀ = 2 nM and murine M109 cellular IC₅₀ = 5 nM), with a human whole blood (hWB) IC₅₀ potency ranging between 2 and 42 nM depending on the donor. It also enhances the proliferation of T_{eff} cells with an EC₅₀ range of 2–7 nM in a human T cell + DC mixed lymphocyte reaction (MLR) assay. Linrodostat was advanced into phase I clinical studies in 2016.^{14a} Currently, linrodostat is in several clinical trials including a phase III study in bladder cancer in combination with nivolumab.^{14b}

More recently, we disclosed the structure of a closely related clinical candidate, BMS-986242 (**5**), which entered phase I clinical trials in 2017.^{14c,d} Preclinical biotransformation studies of BMS-986242 in hepatocytes across several species revealed the formation of metabolites resulting from quinoline oxidation and amide bond cleavage. For this reason, we pursued structurally differentiated IDO1 inhibitors that no longer contained an amide (this work) and/or contained a less metabolically labile replacement for the quinoline. Studies around the quinoline portion of the molecule will be disclosed in due course. Notably, other groups have pursued similar approaches to optimize this chemotype by replacing the amide in linrodostat with an oxalamide.^{15a,b}

A docking pose of compound **4** (Figure 2, shown in magenta) in hIDO1 was modeled based on an X-ray cocrystal

Scheme 2. General Schemes for the Synthesis of Acid Intermediates with Modified R¹ and Quinoline R² Substitution^a



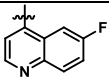
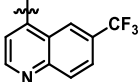
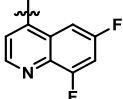
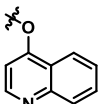
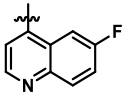
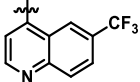
^aReagents and conditions: (a) Pd(PPh₃)₄, K₂CO₃, dioxane, H₂O, 100 °C; (b) Pd–C, MeOH, HCOONH₄, 80 °C or Pd–C, MeOH, H₂; (c) LiOH, H₂O, THF, rt–70 °C; (d) 1,3-dimethyl-3,4,5,6-tetrahydro-2(1H)-pyrimidinone, lithium diisopropylamide, THF, R¹X, –78 °C–rt; (e) NaH, DMSO, 60 °C, 4 h.

structure of compound (**6**) (a closely related analogue is shown in green).^{14c} This model reveals that the chlorophenyl moiety makes an edge-to-face *pi*-stacking interaction with Tyr126. The amide NH forms a key H-bond interaction with Ser167. The cyclohexyl core serves as a rigid scaffold that correctly positions the quinoline and phenyl group in the preferred *cis*-configuration. The quinoline moiety occupies a hydrophobic pocket, and the quinoline nitrogen could form a H-bond with Arg343. These observations provided key insight into the design of new analogues.

Herein, we describe our efforts toward identifying a nonamide-containing IDO1 inhibitor while maintaining potency and improving pharmacologic properties. Heterocyclic amide isosteres have been extensively studied in the literature.¹⁶ Previous examples have shown that five-membered heterocycles can be effective amide isosteres.^{17a,b,18} The success of a given isostere will depend on whether the amide is simply a spacer or if it is taking part in key interactions that are critical to molecular recognition. Given the critical nature of the H-bonding event between Ser167 and compound **6**, it was important to select and tailor an isosteric replacement that would maintain this interaction.

All isosteres discussed can be synthesized via the intermediacy of a carboxylic acid such as previously reported acid **7** (Scheme 1).¹⁹ To obtain oxazole **8** or imidazole **9**, intermediate **7** is coupled with 2-amino-1-(4-chlorophenyl)ethan-1-one. To yield **8**, the resulting amide can be heated in POCl₃ to affect dehydration/cyclization. Alternatively, this amide can be heated with ammonium acetate in the presence of acetic acid to give imidazole **9**. In route to oxadiazole **10** or triazole **11**, intermediate **7** can be treated with *t*-butyl carbazide

Table 2. Effects of R¹ Substitution and Quinoline Modifications to Amino-oxadiazoles on IDO1 Inhibitory Activity, *in Vitro* Metabolic Stability, and PXR Activation

Cmpd #	R ¹	R ²	<i>cis</i> -/ <i>trans</i> -	HeLa / M109 IC ₅₀ μM ^a	hWB IC ₅₀ μM ^a	Metabolic stability (% rem.) (H / M / R) ^b	PXR IC ₅₀ μM ^c (Y _{max})
25	Et-		<i>cis</i> -	0.006±0.002/ 0.031±0.009	0.016±0.007 (N=3)	66 / 31 / 45	0.94 (161%)
26	Et-		<i>cis</i> -	0.003±0.001/ 0.006±0.002	0.050±0.030 (N=4)	83 / 39 / 100	1.06 (132%)
27	Et-		<i>cis</i> -	0.003±0.001/ 0.036±0.024	0.014±0.005	54 / 8 / 52	0.55 (86%)
28	Et-		<i>trans</i> -	0.013±0.003/ 0.148±0.031	0.459±0.250	83 / 39 / 88	>50 (5%)
29	MOM-		<i>cis</i> -	0.003±0.001/ 0.044±0.021	0.031±0.002	57 / 19 / 24	3.03 (34%)
30	EOM-		<i>cis</i> -	0.013 ±0.001/ 0.057±0.033 (N=3)	0.096±0.05	60 / 41 / 53	4.82 (34%)

^aData reported as average of test results (*N* = 2 unless otherwise noted). See Supporting Information for a description of assay conditions.

^bFraction of the parent compound (0.5 μM) remaining after a 10 min incubation with 1 mg/mL of human, mouse, and rat liver microsomes (HLM, MsLM, RLM). ^cThe pregnane X receptor (PXR) transactivation activity was measured by comparing to activation with rifampicin to assess the potential for induction of cytochrome P450 (CYP) 3A4 (Et = ethyl, MOM = methoxymethyl, EOM = ethoxymethyl).

followed by treatment with acid to give a hydrazide (not shown). This hydrazide can be coupled with 4-chlorobenzoic acid and cyclized with POCl₃ to give **10**. Additionally, the hydrazide can be treated with 4-chlorobenzamidine and heated to furnish triazole **11**. Alternatively, the hydrazide can be reacted with 4-methoxyphenylisocyanate followed by cyclization, again with POCl₃, to provide amino-oxadiazole **12**. Amino-oxadiazole **13** could be made in a three-step sequence employing a Curtius rearrangement followed by trapping of the isocyanate intermediate with 4-methoxybenzohydrazide and finally heating in POCl₃ to affect dehydration/cyclization to give **13**. Benzimidazole **14** could be synthesized from **7** by first converting the acid to an acyl chloride and treating with 4-fluoro-1,2-phenylenediamine. Heating the resulting amide with methanesulfonic acid provided benzimidazole **14**.

These various amide isosteres and replacements were evaluated in HeLa (human) and M109 (murine) cellular IDO1 inhibition assays where IDO1 activity can be assessed upon induction with IFN γ (see SI for details). Several five-membered heterocycles were found to be effective replacements for the amide in compound **4** (Table 1). Both imidazole **9** and triazole **11** displayed more potent IDO1 inhibitory activity compared to oxazole **8**. One hypothesis that would account for the greater potency of **9** and **11** is that they maintain a key H-bond donor NH to interact with Ser167. This hypothesis is consistent with the modest potency of oxadiazole **10**. It is of note that **10** is more potent than **8** possibly due to either stronger H-bond acceptor ability or containing two potential H-bond-accepting nitrogens as opposed to one. Analogue **12**, which has an amino linkage between the oxadiazole and aryl ring, displayed a significant

loss of hIDO1 cellular activity compared to **4**. This may be due to the unfavorable orientation of the amino group NH. The “flipped” amino-oxadiazole **13** seems to reorient the NH favorably. Both amino-oxadiazole **13** and benzimidazole **14** demonstrated single-digit nanomolar cellular activity; however, **14** showed inferior metabolic stability.

Based on the cellular potency of amino-oxadiazole **13** and benzimidazole **14**, both were further pursued. Modular synthetic approaches were developed to allow for modification of R¹ and quinoline R² substitution (see Scheme 2). A vinyl boronic acid with R¹ groups preinstalled like **15**^{19–21} (Scheme 2a) could be joined to quinolinyl halides (**16**) with Suzuki coupling. The resulting styrenyl olefin in **17** could be reduced under either transfer or standard hydrogenation conditions and hydrolyzed to give **18** as a mixture of *cis*- and *trans*-racemates. Alternatively, the R¹ group could be installed later in the route by first coupling **16** (Scheme 2b) to unsubstituted boronic acid **19**¹⁹ to give **20**. The position *alpha* to the ester could then be alkylated either before or after reduction of the olefin. Hydrolysis would again give intermediates of type **18**. O-Linked quinolines could be made from *trans*-alcohol **21**^{19,21} employing S_NAr on 4-bromoquinoline **22**. Hydrolysis provides racemic acid **24**. Acids of type **18** and **24** can be converted to amino-oxadiazoles, benzimidazoles, or closely related imidazopyridines as outlined in Scheme 1. All compounds synthesized by the above general methods and discussed in Tables 2 and 3 have been chirally resolved to obtain enantiopure material. For all final compounds discussed in Tables 2 and 3, only the *most potent* enantiomer is shown. To elucidate the relative *cis*-/*trans*-stereochemistry of final compounds or synthetic precursors, ¹H NMR, ¹³C NMR, 2D COSY, 2D NOESY, and ¹H–¹³C–Dept-

Table 3. Effects of R¹ Substitution and Quinoline Modification of Benzimidazoles and Imidazopyridines on IDO1 Inhibitory Activity and *in Vitro* Metabolic Stability

Cmpd #	R ₁	R ₂	<i>cis</i> -/ <i>trans</i> -	X	HeLa / M109 IC ₅₀ μM ^b	hWB IC ₅₀ μM ^c	Metabolic stability (% rem.) ^d (H / M / R)
31	Me- ^a		<i>cis</i> -	C	0.003±0.002/ 0.012±0.007 N=5	0.032±0.008 N=3	48 / 12 / 8
32	Me- ^a		<i>cis</i> -	N	0.004±0.001/ 0.036±0.010	0.026±0.012 (N=3)	67 / 22 / 17
33	Et-		<i>cis</i> -	C	0.002±0.002/ 0.003±0.001	0.009±0.005 (N=3)	82 / 49 / 27
34	Et-		<i>cis</i> -	N	0.002±0.000/ 0.005±0.001	0.006±0.002	78 / 7.0 / 35
35	Et-		<i>trans</i> -	C	0.007 ±0.003/ 0.052±0.010	0.036±0.043 (N=4)	84 / 82 / 80
36	Et-		<i>cis</i> -	N	0.002±0.002/ 0.003±0.002	0.021±0.003	81 / 57 / 81

^aAbsolute stereochemistry is *R*-. ^bData reported as average test results (*N* = 3, unless otherwise noted). See Supporting Information for a description of assay conditions. ^chWB = human whole blood; data reported as average test results (*N* = 2, unless otherwise noted). See Supporting Information for a description of assay conditions. ^dFractions of the parent compound (0.5 μM) remaining after a 10 min incubation with 1 mg/mL of human, mouse, and rat liver microsomes (HLM, MsLM, RLM).

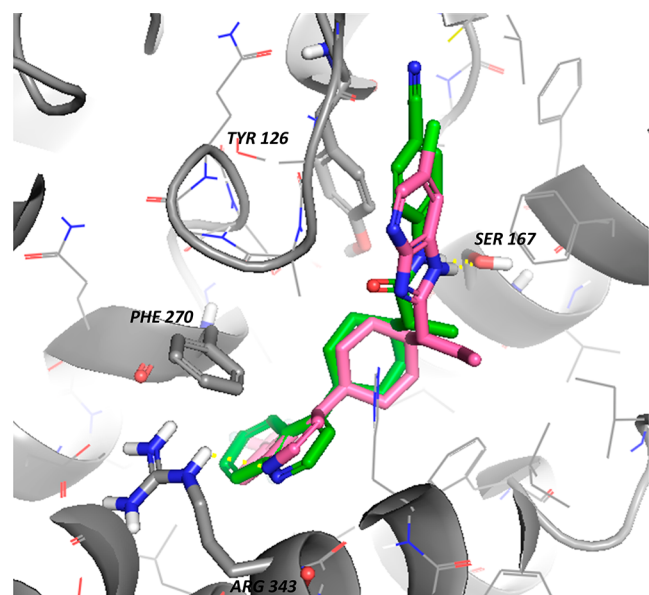


Figure 3. Putative binding mode of compound 36 in hIDO1, based on an X-ray cocrystal structure of compound 6 (green).

HSQC were performed (see SI for details). Absolute stereochemistry was not confirmed unless specifically noted.

Amino-oxadiazoles related to 13 are discussed in Table 2. Introducing an ethyl substituent at the position *alpha* to the ester (25) maintained potency and proved to be beneficial in terms of metabolic stability. Analogue 25 also showed potent hWB activity. Since quinolines are a known potential site of

Table 4. Compound 36 *in Vitro* Profiling

parameter	compound 36
met. stability CYP (<i>T</i> _{1/2} min)	54 (H), 17 (M), 60 (R), 41 (D), 21 (C)
met. stability UGT (<i>T</i> _{1/2} min)	95 (H), >120 (M), 107 (R), 105 (D), >120 (C)
PAMPA cosolvent (pH 7.4)	pH 5.5: 2380 nm/s pH 7.4: 2630 nm/s
caco (a-b:b-a)	113: 66 nm/s
PXR-TA EC ₅₀ (μM)	1.19 (32% <i>Y</i> _{max})
human rCYP panel IC ₅₀ (μM)	1A2: 2.55 2D6: 4.28 2C8: 1.47 2C9: 0.242 2C19: 1.13 3A4: 1.93

Table 5. PK–PD Study of Imidazopyridine 36 vs Linrodostat (4) in a Human SKOV3 Xenograft Tumor Mouse Model

treatment	dose (QDX5) (mg/kg)	PK ^a AUC _{0–24h}	PD ^b AUEC _{0–24h} % [Kyn]↓
linrodostat 4	60	34.9	61
compound 36	20	43.6	56

^aPK is AUC (0–24 h) in tumor μM**h*. ^bPD is percent kynurenine AUEC (0–24 h) reduction. % Kyn reduction was measured at a steady state after the 5th dose in the tumor, calculated as the area under the Kyn concentration–time curve from 0 to 24 h and compared with that of vehicle control.

metabolic oxidation,^{22a} we turned our attention to modeling substituent effects on the oxidation potentials of quinolines.^{22b} Reduction potentials of nitrogen-containing compounds have been reported to correlate with the lowest unoccupied molecular orbital (LUMO) energies.^{23,24} Modeling calculations suggested that electron-withdrawing group(s) on the quinoline ring could reduce N-oxidation potential. For example, 6-CF₃ quinoline displays higher predicted reduction potential $E_{\text{red}} = 2.12$ than that of 6-F-quinoline $E_{\text{red}} = 1.93$.^{22,23} Gratifyingly, the 6-CF₃-substituted quinoline **26** offered potent cellular activity as well as improved metabolic stability but had a 3–4-fold loss of hWB potency compared to analogue **25**. Analogue **27**, with a 6,8-difluoro-quinoline moiety, unexpectedly showed less stability, especially in mouse LMs. Further profiling revealed that all three *cis*-isomers (**25–27**) led to PXR activation. As a consequence of this finding, efforts were focused on improving PXR activity. We were pleased to find that O-linked *trans*-isomer **28** did not activate PXR, but unfortunately it showed not only a 10-fold disparity between human and mouse IDO1 activity, which would hinder *in vivo* studies, but also a significant drop in hWB potency. It is worth noting that the *trans*-isomer of C-linked compound **25** (not shown) also did not activate PXR; however, IDO1 inhibitory activity was very poor. We then turned our attention to *alpha*-substituent modification and found that *alpha*-MOM-substituted analogue **29** and *alpha*-EOM-substituted analogue **30** both demonstrated significant improvement in PXR activity compared to compounds **25–27**. While **29** and **30** maintained good hIDO1 activity in cells, they had more modest hWB potency ($IC_{50} = 0.031 \mu\text{M}$ and $0.096 \mu\text{M}$, respectively, vs $0.002–0.042 \mu\text{M}$ for **4**) and metabolic stability compared to lead compound **4** (see Table 1). Since PXR activation could not be remedied while maintaining suitable hWB and mouse cellular activity, this series was not progressed.

We then focused on the benzimidazole series. Although benzimidazole **14** displayed poor metabolic stability, it had very potent cellular activity (see Table 1). Therefore, identification of a more stable benzimidazole was of primary interest. Addition of a chloro substituent on the phenyl ring of the benzimidazole in combination with incorporation of a nitrogen atom into the ring yielded imidazopyridine **32** (Table 3), which exhibited a significant improvement in stability compared to **31** (H/M/R = 67/22/17) while maintaining hWB activity ($IC_{50} = 0.039 \mu\text{M}$). As was previously observed in the amino-oxadiazole series, introduction of ethyl substitution at the *alpha*-position generally increased potency and improved metabolic stability. Analogue **33** displayed potent hWB activity and improved stability, while imidazopyridine **34** revealed unexpectedly poor mouse metabolic stability (H/M/R = 78/7/35). Consistent with trends observed in the amino-oxadiazole series (see **28**, Table 2), incorporating an O-linked *trans*-isomer (**35**) was found to increase metabolic stability. Once again, however, mouse cellular activity suffered. Combining the more potent *alpha*-ethyl group with the more stable imidazopyridine and the 6-CF₃-quinoline (see **26**, Table 2, *vide supra*) led to compound **36**. Docking models of **36**, based on the X-ray cocrystal of compound **6** and hIDO1 in Figure 2, indicated that the imidazopyridine likely maintains the same key interactions observed for the amide (Figure 3). The NH of the imidazopyridine nicely overlays with the NH of the amide bond in **6** which would correctly position it to make the key hydrogen bond with Ser167. While the pyridine portion of the imidazopyridine is positioned a little lower than

the phenyl ring of **6**, it still is in a position to make a productive edge-to-face *pi*-stacking interaction with Tyr126. Imidazopyridine **36** possessed the best overall *in vitro* profile in terms of potency and stability for this series and was selected for more extensive profiling.

Further *in vitro* profiling (Table 4) showed the compound had modest oxidative metabolic stability; however, this metabolic stability profile was superior to both linrodostat (**4**) ($T_{1/2}$ human = 53, mouse = 4, rat = 20, dog = 17, cyno = 7) and BMS-986242 (**5**) ($T_{1/2}$ human = 14, mouse = 4, rat = 10, dog = 10, cyno = 2). Compound **36** had good intrinsic permeability in a PAMPA assay and Caco-2 cells (a-b = 113 nm/s; efflux ratio = 0.6). Unfortunately, compound **36** showed modest PXR activation (PXR $EC_{50} = 1.2 \mu\text{M}$ (30% Y_{max})) and CYP inhibition in several human isoforms including potent inhibition of CYP 2C9.

Compound **36** was further examined in the SKOV3 human ovarian carcinoma xenograft model (Table 5). In this model, immune-compromised nu/nu nude mice were implanted with SKOV3 cells, and the resulting tumors were allowed to grow for 2 weeks. On day 14, tumor-bearing mice were dosed with imidazopyridine **36** QD at 20 mg/kg for 5 days. On day 18 at 2, 6, and 24 h time points, tumor kynurenine concentration (PD) and compound **36** concentration (PK) were measured in the tumor. The reduction of kynurenine levels, when compared to a vehicle control, was used as a pharmacodynamic marker. Imidazopyridine **36** demonstrated a robust profile. At a 20 mg/kg dose, it achieved 56% reduction in tumor kynurenine levels and tumor exposure of $43.6 \mu\text{M}\cdot\text{h}$ AUC. This profile compares well with linrodostat (**4**): at a 60 mg/kg dose, **4** achieved a 61% reduction in kynurenine levels and a tumor AUC of $34.9 \mu\text{M}\cdot\text{h}$.

In summary, structurally differentiated IDO1 inhibitors were identified. Heterocyclic amide isosteres and replacements were investigated. Amino-oxadiazoles, such as compound **25**, demonstrated potent cellular and hWB potency but led to PXR activation. Optimization of benzimidazole **14** led to the identification of imidazopyridine **36**. Lead compound **36** possessed potent cellular and hWB activity as well as improved metabolic stability ($T_{1/2}$). Additionally, it had a suitable permeability profile. Based on these findings, compound **36** was advanced into an *in vivo* human SKOV3 xenograft tumor model in mice. Compound **36** demonstrated a robust PK/PD profile with improved exposure and comparable PD effects to linrodostat (**4**). In contrast to linrodostat (**4**), which showed less PXR activation (PXR $EC_{50} > 50 \mu\text{M}$ (13% Y_{max})) and a cleaner rCYP panel profile, compound **36** demonstrated more significant PXR activation and CYP inhibition across several isoforms; therefore, compound **36** was not investigated further.

■ ASSOCIATED CONTENT

Supporting Information

The Supporting Information is available free of charge at <https://pubs.acs.org/doi/10.1021/acsmchemlett.1c00014>.

Biological assay protocols, *in vivo* pharmacokinetic–pharmacodynamic study protocols, experimental procedures, and analytical data for all final compounds (PDF)

■ AUTHOR INFORMATION

Corresponding Authors

Liping Zhang – Bristol Myers Squibb Research and Development, Princeton, New Jersey 08543-4000, United

States; orcid.org/0000-0002-1797-7227; Phone: 609-252-3087; Email: liping.zhang@bms.com

Emily C. Cherney – Bristol Myers Squibb Research and Development, Princeton, New Jersey 08543-4000, United States; Phone: 609-252-6064; Email: emily.cherney@bms.com

Aaron Balog – Bristol Myers Squibb Research and Development, Princeton, New Jersey 08543-4000, United States; Phone: 609-252-4632; Email: aaron.balog@bms.com

Authors

Xiao Zhu – Bristol Myers Squibb Research and Development, Princeton, New Jersey 08543-4000, United States; orcid.org/0000-0001-7647-4390

Tai-an Lin – Bristol Myers Squibb Research and Development, Princeton, New Jersey 08543-4000, United States

Johnni Gullo-Brown – Bristol Myers Squibb Research and Development, Princeton, New Jersey 08543-4000, United States

Derrick Maley – Bristol Myers Squibb Research and Development, Princeton, New Jersey 08543-4000, United States

Kathy Johnston-Allegretto – Bristol Myers Squibb Research and Development, Princeton, New Jersey 08543-4000, United States

Lisa Kopcho – Bristol Myers Squibb Research and Development, Princeton, New Jersey 08543-4000, United States

Mark Fereshteh – Bristol Myers Squibb Research and Development, Princeton, New Jersey 08543-4000, United States

Christine Huang – Bristol Myers Squibb Research and Development, Princeton, New Jersey 08543-4000, United States

Xin Li – Bristol Myers Squibb Research and Development, Princeton, New Jersey 08543-4000, United States

Sarah C. Traeger – Bristol Myers Squibb Research and Development, Princeton, New Jersey 08543-4000, United States

Gopal Dhar – Biocon Bristol Myers Squibb R&D Center, Bengaluru, Karnataka 560099, India

Aravind Anandam – Biocon Bristol Myers Squibb R&D Center, Bengaluru, Karnataka 560099, India

Sandeep Mahankali – Biocon Bristol Myers Squibb R&D Center, Bengaluru, Karnataka 560099, India

Shweta Padmanabhan – Biocon Bristol Myers Squibb R&D Center, Bengaluru, Karnataka 560099, India

Prabhakar Rajanna – Biocon Bristol Myers Squibb R&D Center, Bengaluru, Karnataka 560099, India

Venkata Murali – Biocon Bristol Myers Squibb R&D Center, Bengaluru, Karnataka 560099, India

Thanga Mariappan – Biocon Bristol Myers Squibb R&D Center, Bengaluru, Karnataka 560099, India

Robert Borzilleri – Bristol Myers Squibb Research and Development, Princeton, New Jersey 08543-4000, United States

Gregory Vite – Bristol Myers Squibb Research and Development, Princeton, New Jersey 08543-4000, United States

John T. Hunt – Bristol Myers Squibb Research and Development, Princeton, New Jersey 08543-4000, United States

Complete contact information is available at: <https://pubs.acs.org/10.1021/acsmchemlett.1c00014>

Notes

The authors declare no competing financial interest.

ACKNOWLEDGMENTS

We thank Jay Markwalder, Weifang Shan, and the Richard Rampulla/BBRC group for providing intermediates. We thank Dr. Shana Posy for assistance with Figure 3.

ABBREVIATIONS

HATU, 1-[Bis(dimethylamino)methylene]-1H-1,2,3-triazolo-[4,5-*b*]pyridinium 3-oxide hexafluorophosphate; NMM, N-methylmorpholine; DIPEA, *N,N*-diisopropylethylamine; DMF, *N,N*-dimethylformamide; TEA, triethylamine; DPPA, diphenylphosphorylazide; MsOH, methanesulfonic acid; H, human; M, mouse; R, rat; D, dog; C, cyno

REFERENCES

- (1) Adams, J. L.; Smothers, J.; Srinivasan, R.; Hoos, A. Big opportunities for small molecules in immuno-oncology. *Nat. Rev. Drug Discovery* **2015**, *14*, 603–622.
- (2) Austin, C. J. D.; Rendina, L. M. Targeting key dioxygenases in tryptophan-kynurenine metabolism for immunomodulation and cancer chemotherapy. *Drug Discovery Today* **2015**, *20*, 609–617.
- (3) Munn, D. H.; Mellor, A. L. Indoleamine 2,3-dioxygenase and tumor-induced tolerance. *J. Clin. Invest.* **2007**, *117*, 1147–1154.
- (4) Munn, D. H.; Mellor, A. L. Indoleamine 2,3-dioxygenase and metabolic control of immune responses. *Trends Immunol.* **2013**, *34*, 137–143.
- (5) Munn, D. H.; Mellor, A. L. IDO in the tumor microenvironment: inflammation, counter-regulation, and tolerance. *Trends Immunol.* **2016**, *37*, 193–207.
- (6) Prendergast, G. C.; Malachowski, W. P.; DuHadaway, J. B.; Muller, A. J. Discovery of IDO1 inhibitors: from bench to bedside. *Cancer Res.* **2017**, *77*, 6795–6811.
- (7) Yue, E. W.; Sparks, R.; Polam, P.; Modi, D.; Douty, B.; Wayland, B.; Glass, B.; Takvorian, A.; Glenn, J.; Zhu, W.; Bower, M.; Liu, X.; Leffet, L.; Wang, Q.; Bowman, K. J.; Hansbury, M. J.; Wei, M.; Li, Y.; Wynn, R.; Burn, T. C.; Koblisch, H. K.; Fridman, J. S.; Emm, T.; Scherle, P. A.; Metcalf, B.; Combs, A. P. INCB24360 (epacadostat), a highly potent and selective indoleamine-2,3-dioxygenase 1 (IDO1) inhibitor for immuno-oncology. *ACS Med. Chem. Lett.* **2017**, *8*, 486–491.
- (8) Combs, A. P.; Yue, E. W. Preparation of 4-amino-*N*'-hydroxy-1,2,5-oxadiazole-3-carboximidamides and related compounds as modulators of indoleamine 2,3-dioxygenase for inhibiting immunosuppression and treating various disorders. WO 2006122150 A1, November 16, 2006.
- (9) Liu, X.; Shin, N.; Koblisch, H. K.; Yang, G.; Wang, Q.; Wang, K.; Leffet, L.; Hansbury, M. J.; Thomas, B.; Rupar, M.; Waeltz, P.; Bowman, K. J.; Polam, P.; Sparks, R. R.; Yue, E. W.; Li, Y.; Wynn, R.; Fridman, J. S.; Burn, T. C.; Combs, A. P.; Newton, R. C.; Scherle, P. A. Selective inhibition of IDO1 effectively regulates mediators of antitumor immunity. *Blood* **2010**, *115*, 3520–3530.
- (10) Koblisch, H. K.; Hansbury, M. J.; Bowman, K. J.; Yang, G.; Neilan, C. L.; Haley, P. J.; Burn, T. C.; Waeltz, P.; Sparks, R. B.; Yue, E. W.; Combs, A. P.; Scherle, P. A.; Vaddi, K.; Fridman, J. S. Hydroxyamidines inhibitors of indoleamine-2,3-dioxygenase potently suppress systemic tryptophan catabolism and the growth of IDO-expressing tumors. *Mol. Cancer Ther.* **2010**, *9*, 489–498.
- (11) (a) Hamid, O.; Gajewski, T. F.; Frankel, A. E.; Bauer, T. M.; Olszanski, A. J.; Luke, J. J.; Balmanoukian, A. S.; Schmidt, E. V.; Sharkey, B.; Maleski, J.; Jones, M. J.; Gangadhar, T. C. Epacadostat plus pembrolizumab in patients with advanced melanoma: phase 1 and 2 efficacy and safety results from ECHO-202/KEYNOTE-037.

Ann. Oncol. **2017**, *28*, v428–v448. (b) NCT 02752074, ECHO-301/KEYNOTE-252. (c) Mullard, A. IDO takes a blow. *Nat. Rev. Drug Discovery* **2018**, *17*, 307.

(12) Burris, H. A.; Gordon, M. S.; Hellmann, M. D.; LoRusso, P.; Emens, L. A.; Hodi, F. S.; Lieu, C. H.; Infante, J. R.; Tsai, F. Y.-C.; Eder, J. P.; Cleary, J. M.; Jelovac, D.; Tshuhako, A. L.; Mueller, L.; Lin, R.; Morrissey, K.; Mahrus, S.; Morley, R.; Pirzkall, A.; Davis, S. L. A phase Ib dose escalation study of combined inhibition of IDO1 (GDC-0919) and PD-L1 (atezolizumab) in patients with locally advanced or metastatic solid tumors. *J. Clin. Oncol.* **2017**, *35*, 105–105A.

(13) ClinicalTrials.gov Identifier: NCT 02764151: First in patient study for PF-06840003 in Malignant gliomas: <http://www.iteostherapeutics.com/news/20180104-iteos-therapeutics-regains-worldwide-rights-to-clinical-stage-IDO1-inhibitor>.

(14) (a) Balog, A.; Lin, T.-A.; Maley, E.; Gullo-Brown, J.; Hamza Kandoussi, E.; Zeng, J.; Hunt, J. T. Preclinical characterization of Linrodostat mesylate, a novel, potent, and selective oral indoleamine 2,3-dioxygenase 1 inhibitor. *Mol. Cancer Ther.* **2020**, molcancer.0251.2020. (b) A Study of chemo only versus chemo plus nivo with or without BMS-986205, followed by post-surgery therapy with nivo or nivo and BMS-986205 in patients with MIBC. ClinicalTrials.gov. Identifier: NCT03661320. (c) Cherney, E. C.; Zhang, L.; Nara, S.; Zhu, X.; Gullo-Brown, J.; Maley, D.; Lin, T.; Hunt, J.; Huang, C.; Yang, Z.; D'Arienzo, C.; Discenza, L.; Ranasinghe, A.; Grubb, M.; Ziemba, T.; Traeger, S.; Li, X.; Johnston, K.; Kopcho, L.; Fereshteh, M.; Foster, K. A.; Stefanski, K.; Fargnoli, J.; Swanson, J.; Brown, J.; Delpy, D.; Seitz, S.; Borzilleri, R.; Vite, G.; Balog, A. Discovery and preclinical evaluation of BMS-986242, a potent, selective inhibitor of indoleamine-2,3-dioxygenase 1. *ACS Med. Chem. Lett.* **2021**, *12*, 288. (d) An investigational immunotherapy study of experimental medication BMS-986242 given in combination with nivolumab in patients with advanced cancer. ClinicalTrials.gov. Identifier: NCT03351231. (e) Nelp, M. T.; Kates, P. A.; Hunt, J. T.; Newitt, J. A.; Balog, A.; Maley, D.; Zhu, X.; Abell, L.; Allentoff, A.; Borzilleri, R.; Lewis, H. A.; Lin, Z.; Seitz, S. P.; Yan, C.; Groves, J. T. Immune-modulating enzyme indoleamine 2,3-dioxygenase is effectively inhibited by targeting its apo-form. *Proc. Natl. Acad. Sci. U. S. A.* **2018**, *115*, 3249–3254.

(15) (a) Steeneck, C.; Kinzel, O.; Anderhub, S.; Hornberger, M.; Pinto, S.; Morschhaeuser, B.; Albers, M.; Sonnek, C.; Czekanska, M.; Hoffmann, T. Discovery and optimization of substituted oxalamides as novel heme-displacing IDO1 inhibitors. *Bioorg. Med. Chem. Lett.* **2021**, *33*, 127744. (b) Kinzel, O.; Steeneck, C.; Anderhub, S.; Hornberger, M.; Pinto, S.; Morschhaeuser, B.; Albers, M.; Sonnek, C.; Wang, Y.; Mallinger, A.; Czekanska, M.; Hoffmann, T. Discovery of highly potent heme-displacing IDO1 inhibitors based on a spirofused bicyclic scaffold. *Bioorg. Med. Chem. Lett.* **2021**, *33*, 127738.

(16) Meanwell, N. A. Synopsis of some recent tactical application of bioisosteres in drug design. *J. Med. Chem.* **2011**, *54*, 2529–2591.

(17) (a) Kumari, S.; Carmona, A. V.; Tiwari, A. K.; Trippier, P. C. Amide bond bioisosteres: strategies, synthesis, and successes. *J. Med. Chem.* **2020**, *63*, 12290–12358. (b) Mohammed, I.; Kummetha, I. R.; Singh, G.; Sharova, N.; Lichinchi, G.; Dang, J.; Stevenson, M.; Rana, T. M. 1,2,3-triazoles as amide bioisosteres: discovery of new class of potent HIV-1 vif antagonists. *J. Med. Chem.* **2016**, *59*, 7677–7682.

(18) Di Francesco, M. E.; Dessole, G.; Nizi, E.; Pace, P.; Koch, U.; Fiore, F.; Pesci, S.; Di Muzio, J.; Monteagudo, E.; Rowley, M.; Summa, V. Novel macrocyclic inhibitors of hepatitis C NS3/4A protease featuring a 2-amino-1,3-thiazole as a P4 carbamate replacement. *J. Med. Chem.* **2009**, *52*, 7014–7028.

(19) Beck, H. P.; Jaen, J. C.; Osipov, M.; Powers, J. P.; Reilly, M. K.; Shunatona, H. P.; Walker, J. R.; Zibinsky, M.; Balog, J. A.; Williams, D. K.; Markwalder, J. A.; Seitz, S. P.; Cherney, E. C.; Zhang, L.; Shan, W.; Guo, W.; Huang, A. Preparation of immunoregulatory agents. WO 2016073774, May 12, 2016.

(20) Beck, H. P.; Jaen, J. C.; Osipov, M.; Powers, J. P.; Reilly, M. K.; Shunatona, H. P.; Walker, J. R.; Zibinsky, M.; Balog, J. A.; Williams,

D. K.; Guo, W. Immunoregulatory agents. WO 2016073738, A2, May 12, 2016.

(21) Beck, H. P.; Jaen, J. C.; Osipov, M.; Powers, J. P.; Reilly, M. K.; Shunatona, H. P.; Walker, J. R.; Zibinsky, M.; Balog, J. A.; Williams, D. K.; Markwalder, J. A.; Cherney, E. C.; Shan, W.; Huang, A. Immunoregulatory agents. WO 2016073770, A1, May 12, 2016.

(22) (a) Bai, Q.; Yang, L.; Li, R.; Chen, B.; Zhang, L.; Zhang, Y.; Rittmann, B. E. Rittmann. Accelerating quinoline biodegradation and oxidation with endogenous electron donors. *Environ. Sci. Technol.* **2015**, *49*, 11536–11542. (b) Modeling methods for calculating N-oxidation potential: Molecular structures of each model compound are constructed using the Maestro v2015-4 software (Schrodinger, 2015). QM calculations are performed using the Jaguar software (Bochevarov, 2013). Each model compound is subjected to geometry optimization at the B3LYP/6-31G** level of theory and single-point energy calculation at the B3LYP/cc-pVTZ(-f) level of theory, from which the LUMO energy term is extracted. LUMO energy is converted to unscaled reduction potential (eV) via $E_{\text{red}} = -27.2107 * \text{LUMO (hartree)}$ (ref 23) such that higher E_{red} signifies a lower propensity for oxidation.

(23) Assary, R. S.; Brushett, F. R.; Curtiss, L. A. Reduction potential predictions of some aromatic nitrogen-containing molecules. *RCS Advances* **2014**, *4*, S7442–S7451.

(24) Bochevarov, A. D.; Harder, E.; Hughes, T. F.; Greenwood, J. R.; Braden, D. A.; Philipp, D. M.; Rinaldo, D.; Halls, M. D.; Zhang, J.; Friesner, R. A. Jaguar A high-performance quantum chemistry software program with strengths in life and materials sciences. *Int. J. Quantum Chem.* **2013**, *113*, 2110–2142.